Local multifractality in urban systems-the case study of housing prices in the greater Paris region

Janka Lengyel, S G Roux, P Abry, François Sémécurbe, S Jaffard

Local multifractality in urban systems—the case study of housing prices in the greater Paris region

Journal of Physics: Complexity

OPEN ACCESS

PAPER

Local multifractality in urban systems—the case study of housing prices in the greater Paris region

J Lengyel[1,2,*], S G Roux[1], P Abry[1], F Sémécurbe[3] and S Jaffard[4]

[1] ENS de Lyon, CNRS, Laboratoire de Physique, F-69342 Lyon, France
[2] LVMT, Univ Gustave Eiffel, IFSTTAR, ENPC, F-77454 Marne-la-Vallée, France
[3] THÉMA, Université de Franche-Comté, F-25030 Besançon, France
[4] Univ Paris Est Creteil, Univ Gustave Eiffel, CNRS, LAMA UMR8050, F-94010 Créteil, France
[*] Author to whom any correspondence should be addressed.

E-mail: janka.lengyel@ens-lyon.fr

RECEIVED
8 July 2022

REVISED
23 September 2022

ACCEPTED FOR PUBLICATION
4 October 2022

PUBLISHED
28 October 2022

Keywords: local multifractal analysis, inhomogeneous spatial distribution, housing price structure, intra-urban spatial correlations, spectral clustering

Abstract

Even though the study of fractal and multifractal properties has now become an established approach for statistical urban data analysis, the accurate multifractal characterisation of smaller, district-scale spatial units is still a somewhat challenging task. The latter issue is key for understanding complex spatial correlations within urban regions while the methodological challenge can be mainly attributed to inhomogeneous data availability over their territories. We demonstrate how the approach proposed here for the multifractal analysis of irregular marked point processes is able to estimate local self-similarity and intermittency exponents in a satisfactory manner via combining methods from classical multifractal and geographical analysis. With the aim of emphasizing general applicability, we first introduce the procedure on synthetic data using a multifractal random field as mark superposed on two distinct spatial distributions. We go on to illustrate the methodology on the example of home prices in the greater Paris region, France. In the context of complex urban systems, our findings proclaim the need for separately tackling processes on the geolocation (support) and any attached value (mark, e.g. home prices) of geospatial data points in an attempt to fully describe the phenomenon under observation. In particular, the results are indicators of the strength of global and local spatial dependency in the housing price structure and how these build distinct layered patterns within and outside of the municipal boundary. The derived properties are of potential urban policy and strategic planning relevance for the timely identification of local vulnerabilities while they are also intended to be combinable with existing price indices in the regional economics context.

1. Introduction

Multifractal analysis. Multifractal analysis is now considered a standard technique for statistical data analysis [1]. It has been tested in numerous applied settings ranging from medical [2, 3] and satellite image processing [4, 5] to the modeling and prediction of certain natural phenomena [6–9]. In the geographical domain, the core idea is to investigate the spatial complexity and organisation in the city, system of cities and/or urban-rural systems alike, associated with their morphological [10–13], societal [14, 15] and economic structures [16–18]. In more detail, traditional geographical concepts such as that of area, length or density can be replaced by scaling exponents that capture the multiscale codependencies of the latter and may reveal qualitatively new properties in urban structures. Second, a rather well-known and also here-harnessed advantage of multifractal analysis in geospatial settings is that the estimations are largely independent from spatial boundary constraints [14, 16, 18, 19] allowing for an unbiased spatially continuous analysis.

The standard procedure for multifractal analysis involves the computation of the multifractal spectra, where a single scaling exponent is succeeded by a set of scaling indices. It essentially characterizes underly-

ing multiplicative cascade processes—if these exist—where the probability for extreme fluctuations increases with consecutively smaller scales. Even though local coefficients are being oftentimes deployed to derive these global parameters, e.g. on the regional- or city-level, the notion of district-scale *local multifractality* within cities and metropolitan regions is being less often investigated. Latter issue is key for understanding complex spatial correlations within urban regions while the methodological challenge can be mainly attributed to inhomogeneous data availability over their territories. We introduce a novel methodology stemming from concepts and methods used in standard multifractal analysis to define self-similarity and small-scale intermittency in urban systems using two kinds of specifically devised multiscale quantities. A distinct approach is introduced for the support or the spatial location of data points and for its mark, e.g. demographic or economic variables. In such a way, we also demonstrate how the procedure is able to minimize the effects of the spatial distribution on the fractal and multifractal estimation of the mark, ultimately reinforcing a more comprehensive description of the chosen geospatial phenomenon: in complex urban systems in particular such support/mark decoupling could prove instrumental in increasing our understanding of the relationship between the spatial or physical dimension and the social, economic or environmental aspects. Even though the main focus of this article lies on geospatial settings, we must emphasize that the here-proposed method of disentangling the fractal measures of external geometry (inhomogeneous support) from intrinsic multifractality (mark) could be applied to a number of other inhomogeneous complex systems as well. In particular, the important problem of turbulent and non-turbulent fluid flow interfaces [20] as they occur in wall-bounded flows (e.g. pipe or channel flows), wakes in wind parks [21], or the atmospheric boundary layer [22], could be analyzed in more detail by our procedure and may ultimately provide important new insights into the spatio-temporal organization of such complex flows. Further potential areas of applications may include subsurface hydrology [23], neural networks [24] or problems treated by directed percolation [25].

Housing price. Housing price in urban environments is both the symptom and the originator of numerous societal challenges. The interconnected loop of housing affordability, preferential selection of household types and the resulting risk of poverty or social exclusion constitutes a major challenge, especially for larger metropolitan regions. Therefore, the accurate characterization of local housing price structure is an issue of great urban policy and strategic planning relevance with regard to the timely identification of locally vulnerable areas. It is also a potentially valuable tool for delineating intraregional adjustment strategies and orchestrating enhanced local compromises e.g. in the territorially competitive suburban fringes of metropolitan Paris [26, 27]. Prior studies have already linked the (multi-)fractality of home prices to classical measures of economic inequalities and segregation [18, 28], while multifractal interpolation methods have been devised to model the spatial structure of land prices [17, 29]. Even though the real estate market literature emphasizes the role of *neighbourhood-level* spatial spillover effects in influencing housing values [30, 31], there has been less discussion on the distribution of within-city multifractality of housing price and how this relates to other statistical properties of the same dataset, e.g. to those of its support: throughout this paper, by support we refer to the spatial distribution of data points defined by their x and y coordinates. In intraregional contexts in particular, it has been shown that relative difference in real estate prices may contribute to differences in local economic output and significantly affect labor mobility and unemployment [32, 33]. Consequently, not only is a *local analysis* of great relevance but the latter mentioned advantage of fractal analysis, namely its independence from spatial boundary constraints, may be able to capture such spatial dependencies in a largely unbiased manner and lend itself well for neighbourhood-level contexts. Finally, previous research established that housing demand and supply considerably alters real estate transaction values [31, 34], therefore the mark/support decoupling proposed here may constitute an important attempt toward fully describing the nature of correlations in the dataset.

Numerous quantitative models have already been devised to capture the determinants and evolution of housing and commercial property values in the urban economics context. These include, standard [30, 35, 36] and autoregressive hedonic price [37, 38] models, repeat sales models [39, 40] and quantile regression models [41] as well as a combination of these [42–44]. We see the methodology for local multifractal analysis as a complementary approach that could potentially be integrated with the above mentioned models either in a unified or in a more loose composite manner: such efforts may facilitate the introduction of additional valuable information on spatial and temporal interdependencies/effects. Further background on the housing price literature will be provided in the case study section discussing the greater Paris region with more specificity.

Goals. The goal of this research is threefold. The proposed methodology is firstly foreseen to derive the multifractal characteristics of the support (e.g. number and location of purchases) and the mark (e.g. square-meter transaction value) *in a separate manner*. This first research question thus also aims to advance theoretization of the—so far scarcely addressed—influence of these two components on multifractality in complex urban systems. Second, the method must allow for the spatially continuous estimation of neighbourhood-level roughness and intermittency *with sufficing quality* withstanding the fact that local data availabilities may strongly fluctuate over urban territories. Third, in the context of housing prices, it seeks to reveal the strength

of intrascale interdependencies in the price structure and demonstrate how each derived multifractal parameter reveals distinct and relevant information. Moving beyond an aggregate approach, the *local nature* of this analysis intends to clarify how such *interdependencies are distributed within the metropolitan area* under observation—ultimately enhancing planning and policy applicability. Thereby, it also pursues to investigate the strength of their relationship to selected socioeconomic indicators and thus aims at being combinative with other widely used estimation methods of housing price indices, e.g. housing price models in the greater Paris region [30, 35, 42].

Outline. In section 2, we first discuss the dataset and our case study, the greater Paris region and we also revisit relevant research on its housing price structure. Section 3 introduces the methodology for the local multifractal analysis in complex urban systems and provides a comprehensive performance assessment on synthetic data. Section 4 applies the proposed approach to the spatial distribution and value of real estate transactions and gives detailed interpretation of the results. Finally, section 5 foresees to investigate if the derived multifractal parameters may be combined to reveal some *characteristic patterns* in the housing price structure and observes how these complement and relate to other social-economic indicators.

2. Dataset and case study

The dataset used here, 'Demandes de Valeurs Foncières' [45] (property value requests), is made freely available by the official French Directorate General of Public Finances. It provides information on real estate transactions that took place between 2014 and 2020 in metropolitan France and the French overseas departments and territories. The data are derived from notarised deeds on a cadastral resolution and represent the property values as declared at the time of real estate transfers. From this dataset we extract all points that are located within the greater Paris region or the boundaries of the so-called 'Petite Couronne' and the municipal area of Paris, both situated within the Île-de-France department. Altogether the observed area is hosting a population of just below seven million inhabitants (in 2021) and it is made up of the city of Paris and its three bordering departments: Hauts-de-Seine, Seine-Saint-Denis and Val-de-Marne. We must note here that we exclusively analyze housing transactions and for the purposes of this analysis we also cleared data entries of missing values and obvious outliers. In total we obtained 529.784 transaction entries stretching over an area of 762.4 km^2.

In 2020, European Union (EU) households spent an average of 20.0 percent of their disposable income on housing (17.5 percent in France). While within our observation window between 2015 and 2020 the same rate for poor households somewhat declined on the EU scale from 41.7 to 40.2 percent, in France albeit at lower levels, but it was still rapidly rising from 34.9 to 38.2 percent [46]. A study of the Deutsche Bank from 2019 [47] found that in the city of Paris, the monthly rent for a mid-range two-bedroom apartment was the fifth highest in the world, and the corresponding disposable income index rendered the city twentieth least affordable city on a global scale. It thus comes as no surprise that the housing market in and around Paris is profoundly studied in the urban and regional economics literature. In the here relevant intra-regional context, numerous important topics are being addressed ranging from the fundamentals of Parisian housing market dynamics [35] through the study of long-term price convergence between the districts or 'arrondissement' [33] to numerous models for price indices [30, 35, 36, 42]. Among others, the distribution of prices has been investigated in relation to labor market and transport [48, 49], urban amenities [50] and more specifically the distribution of public/private schools [51] as well as social housing [52] and its socioeconomic composition [53]. Our intention is to complement this rich literature with the study of multifractality of housing price to reveal its—so far scarcely addressed—multiscale structural properties on the local level. Since the method intends to reveal several qualitatively new characteristics of the price distribution simultaneously, we believe that the derived parameters may be effectively combined with works carried out by the above studies and models. Finally, we stress that the here utilized dataset is only able to observe characteristics of the 'flexible' part of the so-called dual housing market in Paris as theoreticized by Chapelle *et al* [52] and omits those of the regulated rent sector. Nonetheless, we will bring together our analysis results with social housing features in the final section of this paper.

3. Methodology

The methodology is comprised of two main steps. First, we devise an approach for the analysis of the support and second for the corresponding mark at that location. This differentiation plays an important role in disentangling the effects of the two features, that of the spatial distribution and its attached value on (multi-) fractality, potentially further deepening our understanding of the geospatial phenomenon under analysis. As extensive research already exists on the (multi-)fractal analysis of unmarked point processes in cities, e.g. the size, shape and complexity of urban form [10, 11, 14, 54], the key focus of this paper is dedicated to the second

analytical task. Nevertheless, we believe that it is fruitful to start with the discussion of the support not only to give a coherent overview of the methodology itself but as we will demonstrate, because they also necessitate somewhat different courses of action.

3.1. Multiscale coefficients

To enhance estimation quality, the main difference between the two methodological steps lies in the introduction of differing multiscale coefficients, however in a general sense, subsequent procedure remains analogous and will be discussed in a joint manner in section 3.2.

Support. Starting with the analysis of the spatial distribution of points $e(x_e, y_e)$, determined by their x and y coordinates, we introduce the sand-box coefficient [55] within a ball of radius r, as

$$N(e,r) = \mathrm{card}\{e : d_{e,e'} \leqslant r\}, \tag{1}$$

card standing for the number of observations e. Here, the Euclidean distance between pairs of original point locations e is defined as $d_{e,e'} = \sqrt{(x_{e'} - x_e)^2 + (y_{e'} - y_e)^2}$. It must be noted that we prioritise the sand-box method (equation (1)) over the more commonly used box-counting algorithm [56] for mainly two reasons. Firstly, as our main focus is *local analysis*, it is highly beneficial that the multiscale coefficients of the sand-box framework are already centered on the original observations $e(x_e, y_e)$ themselves. The latter feature means that one will be confronted with less boxes containing solely a few points, thereby avoiding border effects [57] especially problematic at smaller spatial scales. Second, the nature of our data—a marked point process—lends itself well for a 'mass' distribution analysis [57]: we are more concerned with point and value density/intensity characteristics as opposed to e.g. in case of an urban morphological investigation [11] where the extent of covered areas may be of more interest.

Mark. The multiscale quantity $I(e,r)$ of the mark at the corresponding location e will henceforward be defined as the mean of the value $\kappa(e)$ within a radius r,

$$I(e,r) = \frac{1}{N(e,r)} \sum_{e',\, d_{e,e'} \leqslant r} \kappa(e'). \tag{2}$$

It is to be stressed that the difference in the definition between $N(e,r)$ and $I(e,r)$ is crucial, as in case of irregular distributions, it caters for the separation of the two features—support or mark—analyzed and is therefore indispensable for a comprehensive data description. We also note that $N(e,r)$ and $I(e,r)$ are common ingredients of classical multifractal analysis and they are shown to be highly effective for the study of positive measures [14, 58]. With respect to the housing price data studied here, we found that $I(e,r)$ performs significantly better in terms of both estimation quality and support/mark decoupling than a wavelet-based analysis, e.g. where one would substitute $I(e,r)$ by the so-called 'top hat' wavelet coefficient defined for two-dimensional settings as $D(e,r) = I(e,r) - I(e,\sqrt{2}r)$.

3.2. Local multifractal analysis

To derive our local fractal and multifractal parameters we first introduce an equidistant grid with arbitrary lattice size t consisting of points $g(x_g, y_g)$ reaching over the entire observed area. This ensures the spatially continuous estimation procedure across the territory under observation. Secondly, we define a local environment $T > r_{\max}$ ($r_{\max}$ being the largest observed ball of radius r) which is the length scale within which we compute estimations using grid locations $g(x_g, y_g)$ as focal points. The value of T is both dependent on the spatial distribution of the data as well as on the desired resolution for the analysis [59], we also refer the reader to the performance assessment part of this section.

Let $L(e,r)$ henceforth stand for both multi-resolution quantities: $N(e,r)$ of the support and $I(e,r)$ of the mark. To observe local scaling characteristics, this paper uses the cumulants of order one and two however we also define the often used structure functions of moments q as it will be used for observing value-intensity in the following section. In more detail, we define these within the local environment T based on the distance $d_{g,e}$ between estimation sites g and the locations of the original points e as

$$M_q(g,r) = \sum_e w_{g,e} L(e,r)^q \tag{3}$$

$$C_1(g,r) = \sum_e w_{g,e} \log|L(e,r)| \tag{4}$$

$$C_2(g,r) = \sum_e w_{g,e} \big(\log|L(e,r)| - C_1(g,r)\big)^2. \tag{5}$$

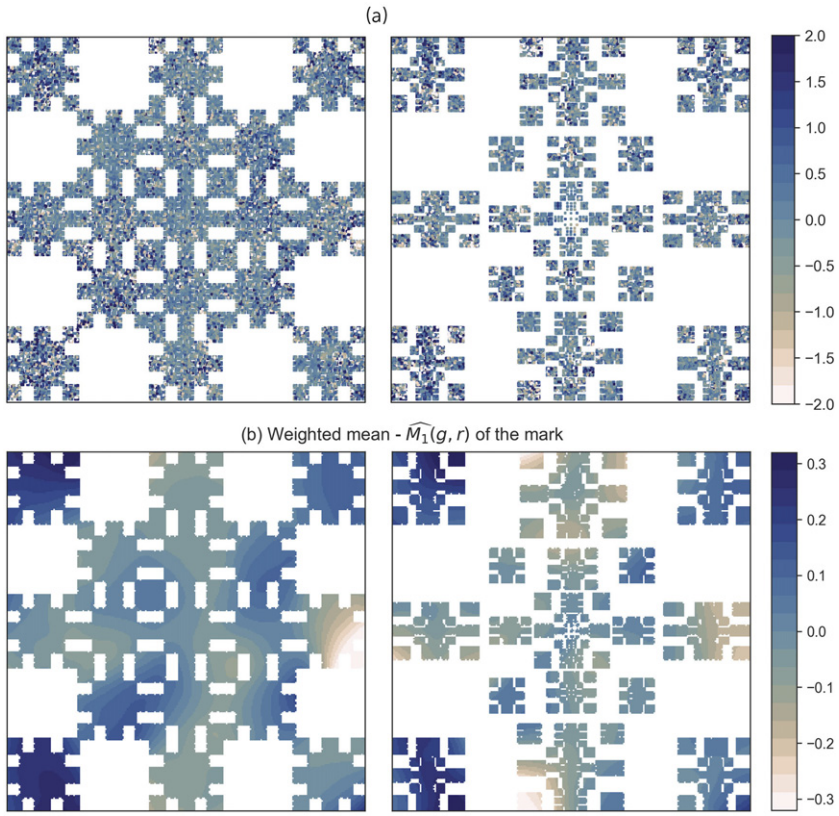

Figure 1. (a) Original point locations $e(x_e, y_e)$ of the homogeneous (left) and non-homogeneous Sierpinski carpet (right) and assigned values of the MRW noise. (b) The weighted mean $\widehat{M_1}(g, r)$ (average value across scales) of the MRW noise value $\kappa(e)$ computed at each grid point $g(x_g, y_g)$.

In all above equations, we use an Epanechnikov kernel weighting function, $w_{g,e} = \frac{3}{4}\left(1 - \left(d_{g,e}/T\right)^2\right)$ if $d_{g,e} < T$ and 0 otherwise, where $d_{g,e} = \sqrt{(x_e - x_g)^2 + (y_e - y_g)^2}$. To derive local value intensities, the weighted mean is defined as $\widehat{M_1}(g, r)$ using equation (3) ($q = 1$) and the coefficient $I(e, r)$. This parameter will prove advantageous to complement the multiscale analysis of local housing price dynamics in the second part of this paper. One can now proceed to recover the local scaling exponents c_1 and c_2 (equations (4) and (5)) by fitting a linear regression using available length scales r. This is performed for each estimation site $g(x_g, y_g)$ and within a local environment T as

$$C_1(g, r) \sim c_1(g)\log(r) + k_1(g) \tag{6}$$

$$C_2(g, r) \sim -c_2(g)\log(r) + k_2(g). \tag{7}$$

In a general sense, $c_1(g)$ is an approximation for self-similarity and the Hurst or self-similarity exponent $H(g)$ is practically very close to $c_1(g)$ as $H(g) \simeq c_1(g) - c_2(g)$, e.g. in case of a log-normal multiplicative cascade. Consonantly, $c_2(g)$ is representative for the level of multifractality and results are considered interpretable if $c_2(g) > 0$ in equation (7). Lastly, we define the global scaling for the entire observed area by computing an average of local scaling functions over all sites g. If $P(g, r)$ stands for each of the two above parameters $C_1(g, r)$ and $C_2(g, r)$ and the total number of estimations sites $g(x_g, y_g)$ is $Q(g)$, the global scaling is obtained as

$$S(r) = \frac{1}{Q(g)}\sum_g P(g, r). \tag{8}$$

Global scaling exponents can then be recovered analogously to those defined for each parameter in equations (6) and (7).

3.3. Performance assessment using synthetic data

To emphasize general applicability to geospatial phenomena of any kind, we start by introducing the local multifractal analysis on a synthetic marked point process using a multifractal random field superposed on two kinds of Sierpinski carpets as shown in figure 1(a). Firstly, we used the iterated function system (IFS) fractal

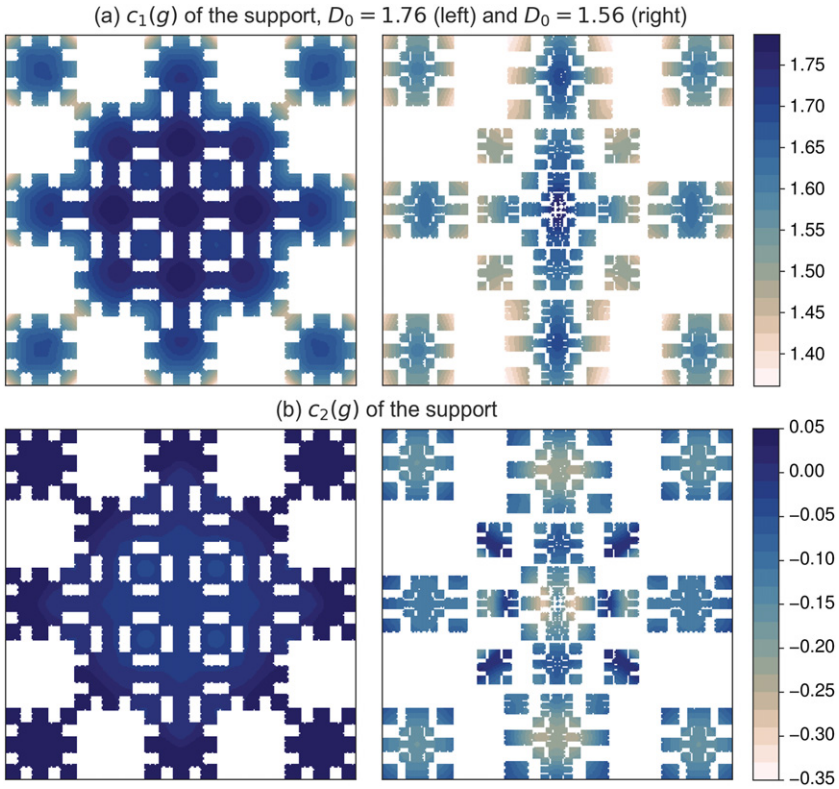

Figure 2. SUPPORT. Cumulant of (a) order one $c_1(g)$, $R_2^{ss} = 0.999$, $R_2^{mf} = 0.996$ and of (b) order two $c_2(g)$, $R_2^{ss} = 0.846$, $R_2^{mf} = 0.821$, using the coefficient $N(e, r)$. The predefined fractal dimensions are $D_0^{ss} = 1.76$ and $D_0^{mf} = 1.56$.

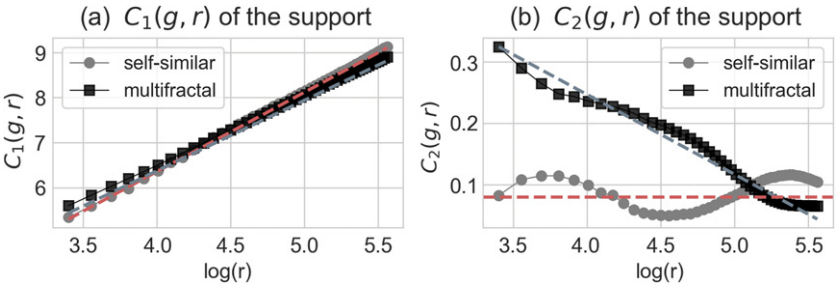

Figure 3. SUPPORT. Scaling of (a) $C_1(g, r)$ and (b) $C_2(g, r)$: we correctly recover (a) predefined fractal dimensions $D_0^{ss} = 1.76$ (red dashed line) and $D_0^{mf} = 1.56$ (blue dashed line) and (b) $c_2^{mf} = -0.125$ (blue) and $c_2^{ss} = 0$ (red).

generator 'GenFrac' [46] to build the carpets, whereby we deployed one ($D_0 = 1.76$, $c_2 = 0$) and then four different ($D_0 = 1.56$, $c_2 = -0.13$) reduction factors to obtain a respective homogeneous and inhomogeneous spatial distribution, with different fractal dimensions $D_0 = -\log(N(e, r))/\log(r)$ and level of multifractality c_2. For clarification purposes, this subsection will use the superscript ss for the self-similar (i.e. homogeneous) and mf for the multifractal (i.e. non-homogeneous) Sierpinski carpet. Note that at a given step of iteration the prefractal Sierpinski carpet obtained has a given nonvanishing area. This is of importance because one can principally think of the previously introduced local multiscale quantity $N(e, r)$ as a proxy for the surface of the prefractal Sierpinski carpet located inside a disk with radius r centered on e. In the sequel therefore, when we refer to a 'mutifractal Sierpinski carpet', it is a shorthand for the multifractal measure supplied by the limit of the sequence of probability measures obtained as follows: one considers the usual 2D support (correctly renormalized) of the prefractal Sierpinski carpet.

Secondly, in order to test the methodology on the mark we need to generate a process with known fractal and multifractal properties. We therefore deploy a widely known multiplicative cascade process, the so-called multifractal random walk (MRW) [60–62], whose multifractal properties are those of the multiplicative log-normal cascade of Mandelbrot [63]. Globally, MRW in figure 1 is a homogeneous, stationary and non-Gaussian process. For more detail on how the 2D field is generated we refer the reader to [7, 64]. In this study, we generate

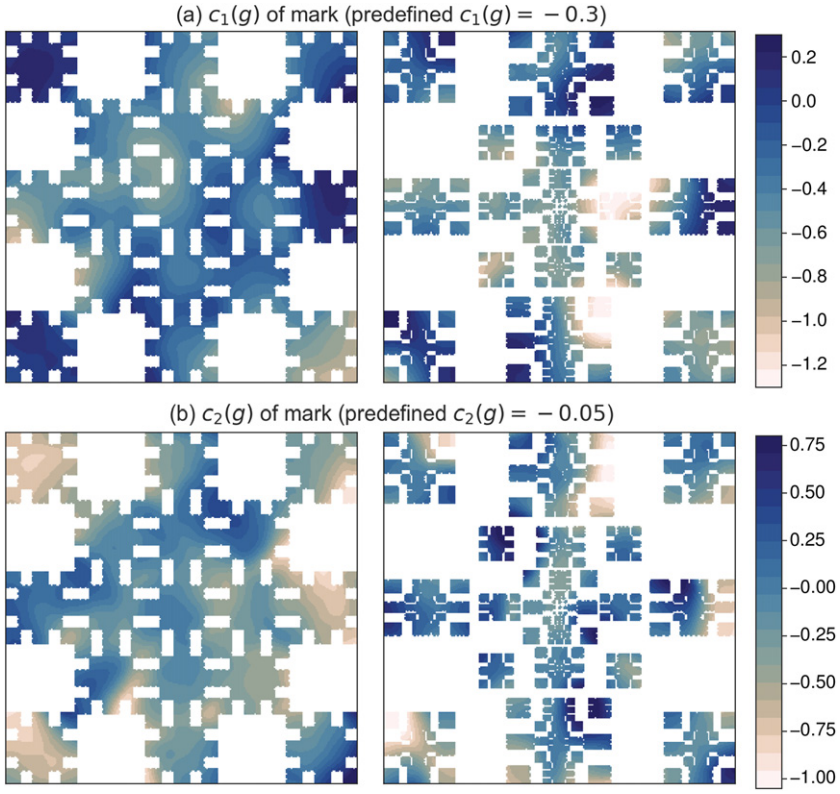

Figure 4. MARK. (a) Scaling exponent $c_1(g)$ (global $c_1(g) = -0.3$), $R_2^{ss} = 0.80$ and $R_2^{mf} = 0.78$, and (b) exponent $c_2(g)$ (global $c_2(g) = -0.05$), $R_2^{ss} = 0.49$ and $R_2^{mf} = 0.38$, of the measure using the multiscale coefficient $I(e, r)$.

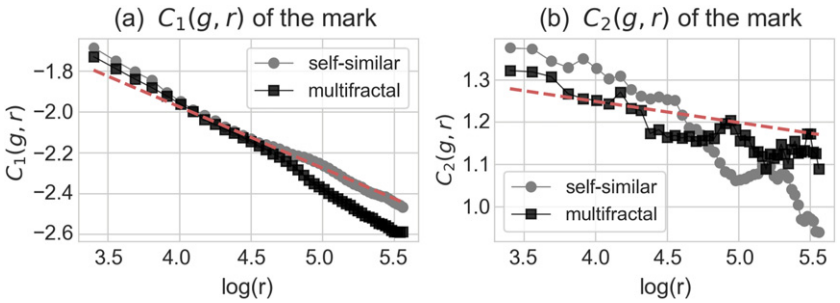

Figure 5. MARK. The scaling of (a) $C_1(g, r)$ and (b) $C_2(g, r)$ using the multiscale coefficient $I(e, r)$ of the mark $\kappa(e, r)$. The slope of red dashed lines correspond to the prescribed values (c) $c_1(g) = -0.3$ and (d) $c_2(g) = -0.05$.

an MRW with a predefined $c_1(g) = -0.3$ and $c_2(g) = -0.05$. With regard to the performance assessment part of the methodological section, we decided for a resolution of $t = 15$ pixels, and we observe the scaling characteristics between $r_{min} = 20$ and $r_{max} = 300$ in 10 px steps, using a larger weighing window $T = 500$ px. Since the original size of our generated images is 4096×4096 px, latter yields a 270×270 resolution for the grid g. To enhance regression quality, we estimate only at those grid points that contain an original point e or where $N(g, \sqrt{2}t) \neq 0$. Finally, all coefficients of determination or R_2 values in this paper are global indicators that are computed for the entire observed area over all estimation sites g as an average.

3.3.1. Results on the support

Starting with the results on the 'support' or the spatial distribution of points $e(x_e, y_e)$, in figure 2(a), local estimations of the cumulant of order one $c_1^{ss}(g)$ and $c_1^{mf}(g)$ fluctuate from grid point $g(x_g, y_g)$ to grid point around the globally defined fractal dimensions $D_0^{ss} = 1.76$ (left) and $D_0^{mf} = 1.56$ (right). Concurrently, the prescribed global scaling (equations (4) and (5)) of the two Sierpinski carpets, indicated with red and blue lines in figure 3(a), can be in average correctly recovered by our proposed methodology for both the self-similar (grey) and multifractal (black) distributions, i.e. the dots are in agreement with predefined scaling indicated

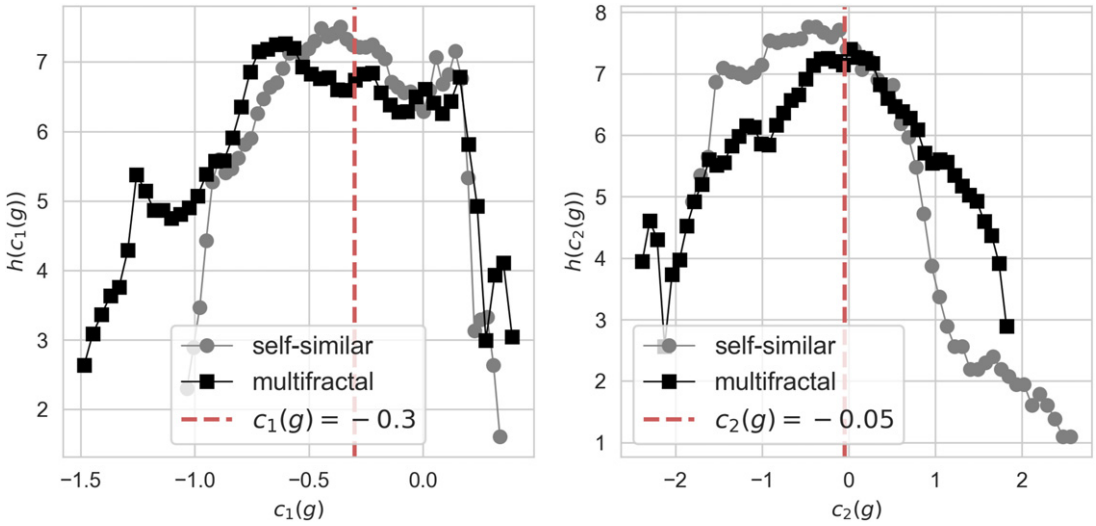

Figure 6. MARK. Histogram of $c_1(g)$ (left) and $c_2(g)$ (right) using the multiscale quantity $I(e, r)$. Red dashed lines indicate prescribed values (left) $c_1(g) = -0.3$ and (right) $c_2 = -0.05$.

with dashed colored lines. The coefficient of determination R_2 lies above 0.995 in both cases. Figure 2(b) displays estimations for c_2 or for the multifractality of the support. As expected, in the left image—showing the homogeneous distribution—it is uniquely the dark blue color or $c_2^{ss} \simeq 0$ that is dominating while this is also confirmed on the scaling in figure 3(b) with $c_2^{ss} = 0$. In contrast, figure 2(b) right displays much larger range of local fluctuations ($-0.35 \leqslant c_2^{mf} \leqslant 0.05$) and for the global scaling exponent in figure 3(b) (blue dashed line) we obtain the predefined $c_2^{mf} = -0.125$. Again, note that this behavior is in line with the theory of multifractal systems where $C_2(g, r)$ decreases with increasing length scales r. In terms of performance, estimation quality for the multifractal exponent $c_2(g, r)$ somewhat declines to $R_2^{ss} = 0.846$ and $R_2^{mf} = 0.821$.

3.3.2. Results on the mark

Let us start with a mathematical clarification: in general, there is no well defined procedure for taking the trace of a measure on a fractal set and deriving a non-trivial result (indeed the simple consideration of the measure of the fractal set will usually yield 0). The procedure we consider here is different: we start with the prefractal Sirpinski carpet at a given level of iteration, which has a piecewise affine boundary, so that the trace is well defined. We consider the restriction of the measure to this set; and when the iteration step in the construction of the Sierpinski carpet increases, we look for the invariant scaling properties of this (correctly renormalized) sequence of measures. Moving on to consider results on this 'measure' or the MRW value superposed at each corresponding centroid point of the Sierpinski carpets (see figure 1(a)). In figure 4(a), local estimation of self-similarity exponents are of sufficient quality ($R_2^{ss} = 0.80$ and $R_2^{mf} = 0.78$) and fluctuate around the predefined $c_1(g) = -0.3$. Similarly to the support, quality declines for multifractalilty $c_2(g)$. Notwithstanding, in figure 6 we deduce that the histograms of $c_1(g)$ (left) and $c_2(g)$ (right), both peak in the vicinity of the prescribed values displayed in red dashed lines. Note that even though the global scaling of $C_1(g, r)$ in figure 5(a) decreases with increasing radii, locally we find both positive and negative scaling exponents $c_1(g)$ (see also figures 6 and 4(a)), a tendency that will also be replicated by the housing price example in the next subsection. As suggested by visual inspection, the obvious difference between figure 2 (support) and figure 4 (mark) propound that results on the mark are largely independent of their underlying point distributions while this is also clearly seen on the close proximity of the two histograms in figure 6: estimations of the mark for the self-similar Sierpinki shown in grey largely coincide with those of the multifractal carpet in black, suggesting that *the two rather distinct spatial distribution of the data points (support) did not significantly affect the roughness and intermittency estimations of the attached MRW values (mark)*. Correlations between the above multifractal parameters will be addressed in greater detail in section 4.

4. Local multifractal analysis of real-world transaction values

The purpose of this section is to first investigate if the devised approach that was previously illustrated on synthetic data may also remain valid on the chosen real-world housing price example. In analogy to figure 1(a), the original real-world point process is displayed in figure 8(a). Location of the purchases that were being made between 2014 and 2020 constitute the 'support' while the 'mark' is the corresponding square-meter

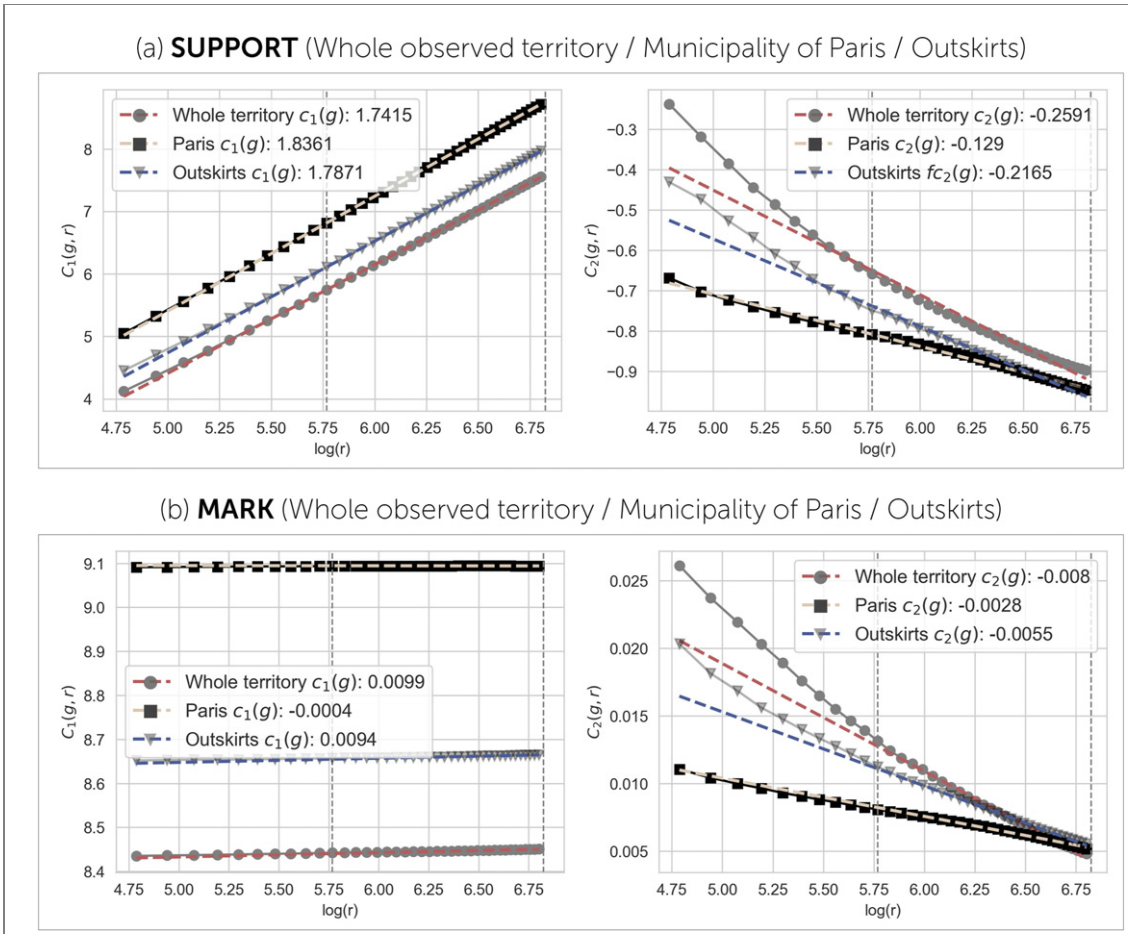

Figure 7. SUPPORT (a) and MARK (b). Comparison of scaling characteristics between the three spatial territories: the entire observed area, the municipality of Paris, and the outskirts of Paris (two whole Petite Couronne area except from grid points g located within the Paris municipality). Scaling of (a) $C_1(g,r)$ and $C_2(g,r)$ of the support and (b) $C_1(g,r)$ and $C_2(g,r)$ of the mark.

transaction value, shown here on a logarithmic scale. The weighted mean $\widetilde{M_1}(g,r)$ of housing price is displayed in figure 8(b) (corresponding to figure 1(b) from the methodology section of this paper) building a well-known radial structure where price decreases with distance from the city center.

Global analysis. Before proceeding to examine the results of the local multifractal analysis, it is important to investigate the global behavior of the four scaling functions using equation (8). The goal is thereby to recover characteristic scaling schemes as an average over the observed territory, that will ultimately help us to define the radii r for the local analysis. Figure 7(a) shows the global scaling of the support and figure 7(b) the global scaling of the mark between 20 and 840 m in 20 m steps. It is widely evident that intermittency exponents $c_2(g)$ of the support and the mark (figure 7 right column) are manifesting two distinct scaling regimes: (i) a characteristic scaling behavior at small scales up until around 240 m, and (ii) between approximately 240 and 840 m. A local linear regression fit for the $c_2(g)$ exponent of the mark at small scales (i) revealed that the behavior of $C_2(g,r)$ at this scaling regime is highly influenced by, and is therefore largely in line with the multifractality of the support $C_2(g,r)$. The latter can be attributed to insufficient data availability at (i) rendering the separation of the two processes yet inaccessible. Accordingly, in the following part of this paper we will conduct our analysis at scaling regime (ii) as indicated with gray dotted lines in figure 7. A more detailed account of the global scaling exponents is given in the following section. A corresponding larger local environment $T = 1200$ m is then chosen to reduce boundary effects [14, 65], while for the estimation grid we decided for a resolution of $t = 100$ m. We emphasize that the selected resolution for the real-world data yields a comparable—even somewhat improved—data availability to the one used for the MRW process. Let us now progress to observe the local multifractal properties of housing prices in an analogous manner as we did with the synthetic data in the methodology section of this paper.

4.1. Analysis of the 'support' or the spatial distribution of real estate transactions

The $c_1(g)$ exponent for the spatial distribution of purchases is shown in figure 8(c) (this being analogous to figure 2(a)). For the computation we used the sand-box coefficient $N(e,r)$ and we find that the average coefficient of determination is highly sufficient with $R_2 = 0.999$ for the entire observed territory in average.

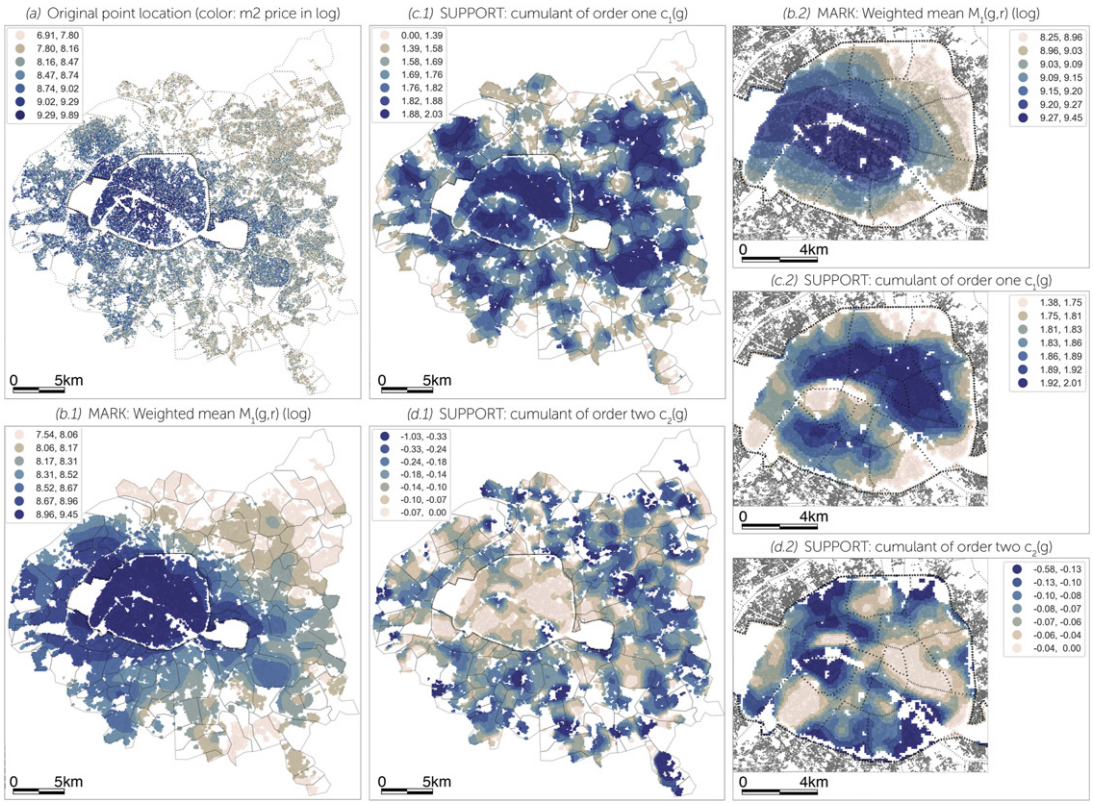

Figure 8. SUPPORT. (a) Location $e(x_e, y_e)$ of the 529.784 purchases analyzed here (taking place between 2014 and 2020) colored by the log of the measure $\kappa(e)$, defined as the square-meter housing price. (b.1) and (b.2) Log of the weighted average $M_1(g, r)$ of the measure $\kappa(e)$ using $I(e, r)$, mean value across available length scales r. (c.1) and (c.2) Cumulant of order one c_1 computed for the support using multiscale coefficients $N(e, r)$. $R_2 = 0.999$ for the entire observed field (c.1) in average. (d.1) and (d.2) Cumulant of order two c_2 of the support using multiscale coefficients $N(e, r)$, $R_2 = 0.889$. Thick black line: municipal boundary of Paris. Thin black line: the communes of Petite Couronne (a.1) and (b.1) and the districts of Paris (a.2) and (b.2).

One maintains that the darker the blue color or the larger the exponent $c_1(g)$, the higher the local concentration and the stronger the interdependence between purchase locations across length scales r. As an example, one may observe that as opposed to the south of the Seine river, the northern parts of Paris are profiting in average of somewhat more pronounced territorial availabilities and/or popularity. There also exist certain clear 'local hotspots' in the suburbs such as for example the dark blue areas north of the boundary of the 'Bois de Vincennes' park located in the twelfth district. The multifractality $c_2(g)$ of the spatial distribution of purchases is displayed in figure 8(d) and its correlation to $c_1(g)$ lies at 0.33. Despite the fact that the global intermittency exponent for purchase locations is rather high $c_2(g) = -0.259$ (figure 7(a)), we nonetheless obtain *sufficing estimation quality* for the so far hard to access local estimations of intermittency at $R_2 = 0.889$. Darker areas reveal higher levels of multiftactality and therefore an increasing probability for extreme local fluctuations in purchase densities at successively smaller scales. A notable SE-NW belt is being revealed ranging from the thirteenth to the seventeenth districts—also crossing the prominent first, sixth and seventh—dotted by rather stark fluctuations of local availabilities. Among others, it is here that the 2014–2018 surge of homebuilding [66] in and around Paris appears to exhibit its strongest spatial correlations in the local sense, a detailed inspection of which however remains for future work. The next subsection will compare these results that addressed the *geolocation* of purchases to the multifractal properties of the *transaction value* attached to them.

4.2. Analysis of the 'mark' or housing price

Before observing the properties of the mark in detail, let us compare these results to those of the support in the global sense. Table 1 shows the Pearson correlation coefficients between the five computed parameters. We find that both of the relationships are of very low amplitude with -0.041 for the self-similarity—i.e. between $c_1(g)$ support and $c_1(g)$ mark—and 0.18 for the multifractal—i.e. between $c_2(g)$ support and $c_2(g)$ mark—exponents. The correlation between the self-similarity exponent and intermittency of price is likewise rather low at -0.29. Relevance of these findings are twofold. First, they now allow for investigating

Table 1. Pearson correlation coefficients between the multifractal parameters of the support (transaction location) and the mark (square-meter transaction value). *Supp.*: support.

	$c_1(g)$ (supp.)	$c_2(g)$ (supp.)	$c_1(g)$ (price)	$c_2(g)$ (price)	$\widehat{M_1}(g,r)$ (price)
$c_1(g)$ (supp.)	1				
$c_2(g)$ (supp.)	0.33	1			
$c_1(g)$ (price)	−0.041	−0.022	1		
$c_2(g)$ (price)	0.12	0.18	−0.29	1	
$\widehat{M_1}(g,r)$ (price)	0.35	0.34	−0.19	0.24	1

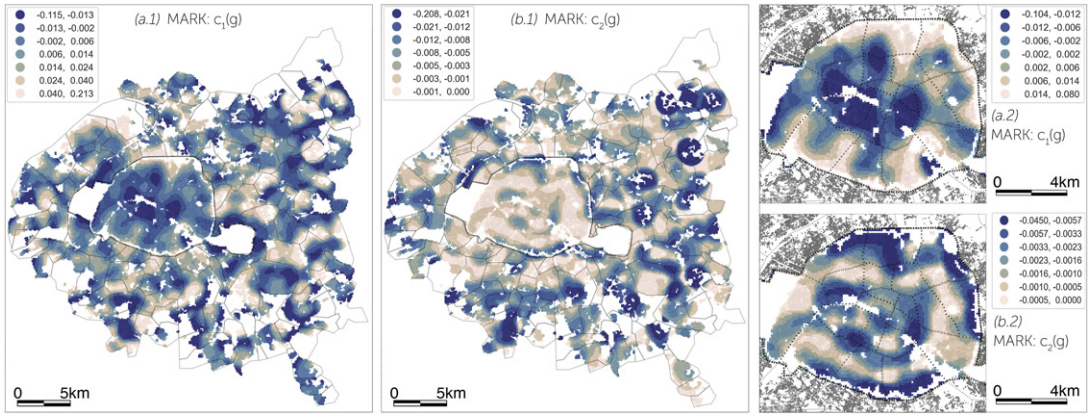

Figure 9. MARK. (a.1) $c_1(g)$ computed for the housing price using multiscale coefficients $I(e,r)$ ($R_2 = 0.763$). (b.1) Cumulant of order two $c_2(g)$ computed for the mark using $I(e,r)$ ($R_2 = 0.881$). (a.2) and (b.2) Corresponding values $c_1(g)$ (a.2) and $c_2(g)$ (b.2) displayed and reclassified solely for the municipality of Paris. Thick black line: municipal boundary of Paris. Thin black line: the communes of Petite Couronne (a.1) and (b.1) and the districts of Paris (a.2) and (b.2).

the multifractality of the two subsystems—that of the support and the mark—in a decoupled manner. Second, they suggest that the five obtained parameters do indeed carry complementary but also rather disparate information. Concerning the parameters $c_1(g)$ ($R_2 = 0.763$) and $c_2(g)$ ($R_2 = 0.881$) of the mark we delineate two general trends: while in general $c_2(g)$ decreases with distance from the city center, $c_1(g)$ is increasing. This signifies simultaneously increasing intermittency and long-range dependency in the data. In other words, the strength of the correlations across multiple scales (hence the structuredness) increases, both in the global ($c_1(g)$) and local sense ($c_2(g)$), as one progresses toward the suburbs. From a spatial economic perspective, these trends point toward homogenisation tendencies in the real estate market within the city of Paris, note also how the dark blue color or the lowest $c_1(g) < -0.006$ values (figure 9(a.2)) are dominating over the entire central municipal area. Similar values of the self-similarity exponent c_1 of housing price—as observed here—are also supported by a recent study in the Ruhr area, Germany [17] while the long-term stationarity of pair-wise land price increments in between Parisian districts has been addressed in [33]. What is interesting to emphasize is that the characteristic radial structure that is to be clearly seen in figure 8(b) ($\widehat{M_1}(g)$) and largely echoed in figure 9(a) ($c_1(g)$), are being periodically 'interrupted' by the intermittency $c_2(g)$ of the price in figure 9(b). These rings of high intermittency (see also figure 9(b.2)) are largely corresponding to the wide boulevards that cut through and border the city, whereas in this case, they also appear to be the intermediaries between different price regimes. The section that follows will continue to discuss the multifactality of price in great detail amongst others in the context of its relationship to certain selected social-demographic indicators.

5. The multifractal housing price structure of the greater Paris region

This section deploys a spectral clustering algorithm on the four multifractal parameters and the weighted mean of housing price in the greater Paris region. The main objective is to observe their interdependency with one another and with a selection of social and economic variables using external census data from the French National Institute of Statistics and Economic Studies (INSEE [67]). The flexibility of such similarity based clustering methods—as the spectral clustering—is rather favourable for our current analysis: it utilizes the connectivity approach that makes no *a priori* assumptions on the shape or distribution of the data thereby rendering it attractive for jointly observing the attributes of a highly irregular spatial distribution (support) and an attached price value (mark). We defined the optimal number or clusters using the elbow method and the altogether seven resulting clusters are displayed in figure 10. In general, the upper bar diagram and table 2

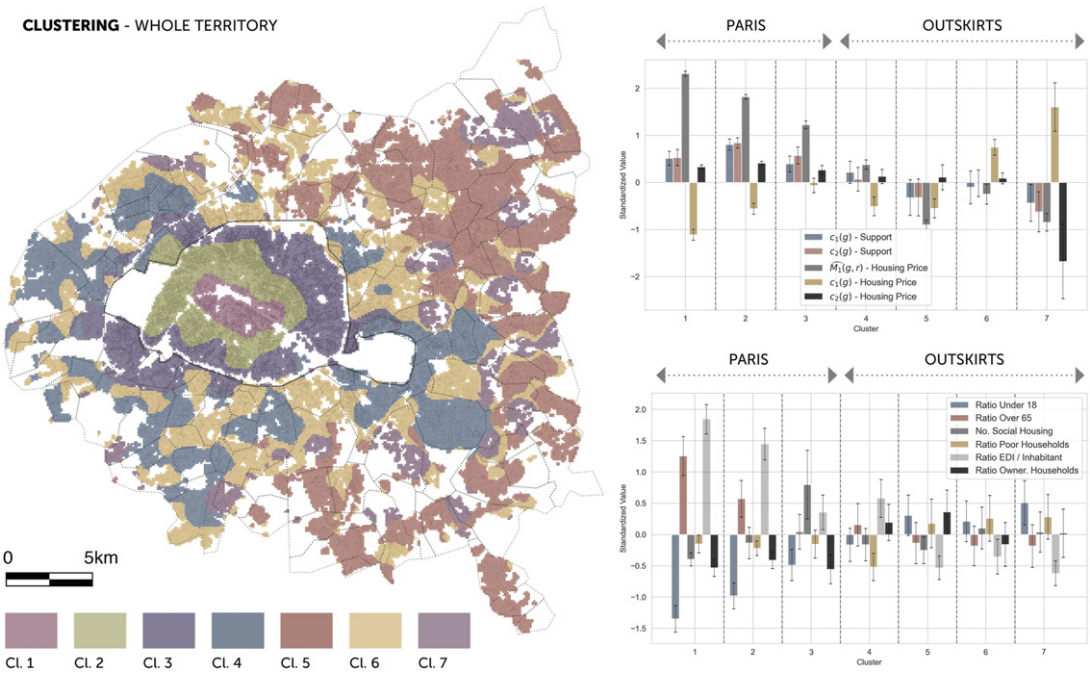

Figure 10. Spectral clustering results (left) using five features: $c_1(g)$—support, $c_2(g)$—support, $c_1(g)$—price, $c_2(g)$—price, $\widehat{M_1}(g,r)$—price. The bar plots (right) display the average of the regionally standardized values for selected multifractal parameters (top) and socioeconomic indicators (bottom) per cluster. Abbreviations: Cl.: Cluster.

Table 2. Parameters used for the spectral clustering: linear regression is fitted for each scaling function and cluster. The first two columns are the self-similarity and intermittency exponents of the support ($c_1(g)$, $c_2(g)$) while the third and fourth show the same for the mark ($c_1(g)$, $c_2(g)$). The last column displays the log of the weighted mean of the square-meter transaction value per cluster ($\widehat{M_1}(g,r)$). Supp.: support, m.: mark, cl.: cluster.

	$c_1(g)$ (supp.)	$c_2(g)$ (supp.)	$c_1(g)$ (m.)	$c_2(g)$ (m.)	$\widehat{M_1}(g,r)$ (m.)
Cl.1	1.8226	−0.1056	−0.0162	−0.0031	9.35
Cl.2	1.8699	−0.0732	−0.0045	−0.0020	9.16
Cl.3	1.8042	−0.1004	0.0069	−0.0040	8.94
Cl.4	1.7731	−0.1535	−0.0032	−0.0060	8.61
Cl.5	1.6771	−0.1912	−0.0040	−0.0061	8.12
Cl.6	1.7233	−0.1609	0.0249	−0.0064	8.40
Cl.7	1.6843	−0.2221	0.0436	−0.0307	8.15

corroborate our observations form the last subsection (see also the example of global scaling exponents in figure 7) and illustrate well one of the key findings of the local multifractal analysis: in the context of the housing price, both self-similarity ($c_1(g)$) and intermittency (absolute values of $c_2(g)$) increase with distance from the central (-western) parts of the city, while average price ($\widehat{M_1}(g,r)$) decreases. In contrast, with respect to the support we observe that as the strength of *global long-range dependency or regularity* ($c_1(g)$) in the support or the location of transaction values decreases, the strength of intermittency or the level of *local structuredness* in the data increases. Taken together, this diverging multifractal behavior of the support and the mark further underlines the decoupling efforts presented here.

It is to be noted that in terms of the multifractal properties of the support we observe a continuous change in values from Cl.1 through Cl.2, Cl.3 and Cl.4 to Cl.6 while Cl.5 and Cl.7 are well-separated from the latter five clusters (see also table 2): the latter two cover lower-density structures that are often dotted by large-scale commercial and industrial areas. With regard to the multifractal parameters of the price a gradual progression from Cl.1 to Cl.5 is apparent while Cl.6 and Cl.7 (and partly Cl.3) manifest somewhat diverging behavior which will be interpreted in detail in the following paragraph.

After combining our clustering results with the micro-level census data INSEE [67] and calculating the mean value for certain selected variables for each cluster (displayed in the bottom bar diagram in figure 10 and

Table 3. Socio economoic composition of the seven clusters: mean of the ratio per cluster. For social housing we display the mean of regionally standardized values. Freely available micro-level data is downloaded from the official website of the French National Institute of Statistics and Economic Studies (INSEE [67]), only available for the year of 2015. R.: ratio, Soc. H.: Social Housing, H.h.: Households, I.: Inhabitants, EDI: Equivalised Disposable Income (in Euros).

	R. Under 18	R. Over 65	**Soc. H.**	R. Poor H.h.	**R. EDI/I.**	**R. Owner H.h.**
Cl.1	0.1555	0.2277	−0.1992	0.1289	43 181.30	0.3728
Cl.2	0.1763	0.1851	0.1613	0.1227	39 672.29	0.4070
Cl.3	0.2054	0.1514	1.4392	0.1297	30 121.67	0.3685
Cl.4	0.2243	0.1595	0.1025	0.0894	32 467.41	0.5762
Cl.5	0.2502	0.1420	−0.0181	0.1547	22 618.07	0.6232
Cl.6	0.2453	0.1384	0.4641	0.1646	24 204.36	0.4831
Cl.7	0.2619	0.1386	−0.3761	0.1661	21 807.04	0.5290

in table 3), we obtain the following overarching tendencies: characteristic demographic trends are being widely apparent with increasing number of households with children and decreasing above-65 year-olds toward the suburbs. In general the ratio of poor households also increases, however this trend is being occasionally interrupted, for instance in the case of Cl.3 and Cl.4. Here, despite the fact that Cl.3 is still located within the municipal boundary, it can be characterized by larger proportions of poor households (12.97%) than its more affluent neighbor Cl.4 encircling the city (8.94%) and expanding toward the western areas of Petite Couronne. This suggests that similar to other European metropolitan regions, spatial dependency of price and demographic indicators are revealing more and more heterogeneous trends throughout the suburbanization process [68]. Consequently, *local spatial effects*—as they are also addressed here—are gaining ever more importance. For more clarity, we now progress to separately consider *(i)* the first three clusters that are predominantly located within the city of Paris and *(ii)* the four suburban clusters. It is important to mention that the separation of these two groups can partly be attributed to the location of the so-called 'Le boulevard périphérique de Paris', a major ring road of 35.04 km length encircling the city. Le Périphérique is often regarded as a separating artery between the social, economic and cultural milieus of Paris and its suburbs and it is the main target of various urban design and planning schemes that aim at reintroducing urban continuity [69].

(i) Cl.1, Cl.2 and Cl.3 follow the widely studied characteristic radial structure of Parisian price distribution (e.g. in [51, 53, 70, 71] see also the case study section of this paper) that is being tilted toward the west and continues to spill over into the suburbs. Complementary to these interpretations, we maintain that upper-status clusters of Cl.1 and Cl.2 located in and around the touristic old center, are also exhibiting the weakest multiscale spatial correlations in their price structure, i.e. Cl.1 having the lowest $c_1(g) = -0.0162$ and one of the highest $c_2(g) = -0.0031$ according to table 2. These pinpoint to a greatly saturated market reinforced by the presence of the most lucrative properties in the greater Paris region (largest $\widehat{M}_1(g,r) = 9.34$ and $\widehat{M}_1(g,r) = 9.18$). With regards to the support, in the observed time window between 2014–2020, Cl.1 has the highest intermittency exponent $c_2(g) = -0.1056$ thus rapidly intensifying fluctuations across scales in its local housing availability suggesting a highly inhomogeneous distribution. As an example, this finding already signals that the separation of mark from its support is rather relevant: while Cl.1 has comparably low intermittency for the price the opposite is true for the spatial distribution of purchases. *Methodologies that do not specifically target the separation of these two processes may thus yield somewhat skewed results.* In contrast with these trends, the most outer cluster Cl. 3 exhibits by far the strongest spatial interdependencies in the context of its transaction values thus also the highest level of multifractality (lowest $c_2(g) = -0.004$). Since multifractality of price has already been linked to housing inequalities [16, 18], it is interesting to observe how $c_2(g)$ relates to certain social-demographic variables within the city of Paris using the aforementioned micro-level census data. We find that even though prices in average are regionally still very high, in the municipal context Cl.3 has the lowest disposable income rate per inhabitant, highest ratio of under-18 year-olds and number of social housing units (see table 3). Against this background, the excessive price intermittency of Cl.3 appears to be in correspondence with the also here located formerly working-class districts that are being incrementally permeated by middle and upper-class social groups and become increasingly gentrified [53]. These results are in alignment with findings from previous studies, however for the purposes of this paper it is now compelling to determine the extent to which the multifractality of price and socioeconomic variables correlate on the cluster level: we find that a multiple regression model that uses four of the six selected census parameters (indicated with bold text in table 3, $p < 0.001$) as explanatory variables is able to explain 82.5% of the variance in our dependent variable, the $c_2(g)$ of price in Cl.1, 87.2% in Cl.2 and 70.6% in Cl.3. In other words, *social economic parameters are statistically significant in estimating* $c_2(g)$, suggesting that the multifractlity of price does in fact hold impor-

tant complementary information to that of the widely studied mean transaction value. For example, in Cl.3 we deduce that as the disposable income per inhabitant increases by 1, $c_2(g)$ will increase by 0.1883 (thus intermittency decreases) and when the ratio of under 18 year-olds increases by 1, $c_2(g)$ will decrease by -0.1184 (intermittency increases). Even though further detailed multiple regression modeling is beyond the scope of this paper, we included the regression results for the three Parsisian clusters, Cl.1, Cl.2 and Cl.3, in appendix A.

(ii) Cl.4 is by far the most prominent suburban cluster with a closely coexisting maximal price $\widehat{M_1}(g,r) = 8.61$ and minimum intermittency $c_2(g) = -0.006$, but at the same time the highest spatial correlation $c_1(g) = 1.7731$ in the distribution of purchases. Even though amongst *(ii)* clusters the presence of under-18 year-olds is here the lowest, it is still more than four percent higher than the average value within the city of Paris. Latter renders this area a favourable destination for more socially privileged families where upper status from the city continues to expand into the suburban fringes [71]. Furthermore, Cl.4 presents the highest consistency—or $c_1(g)$—in the placement of purchases, making it a competitive residential destination that is also being mirrored by the latter mentioned high average price $\widehat{M_1}(g,r)$. Cl.6 is another interesting example as it fills the voids between its substantially more affluent counterpart Cl.4. Accordingly, it is represented by the second highest $c_1(g)$ and intermittency $c_2(g)$ (second highest absolute $c_2(g)$ value) with respect to home prices in the entire Petite Couronne region. At the same time, it also contains a large share of poor households and the highest number of social housing units in *(ii)* and may thus be *particularly susceptible of imminent gentrification tendencies*. The profile of Cl.5 exhibits somewhat milder correlations in its price structure however still very high intermittency both in its price $c_2(g) = -0.0061$ and underlying support $c_2(g) = -0.1912$ along with regionally lowest prices $\widehat{M_1}(g,r) = 8.12$. Cl.5 areas coincide with traditionally more marginalised working class neighbourhoods that also host a large share of immigrant populations from Maghreb and South-Sahara Africa [53, 71]. Cl.7 appears to cover the somewhat more affluent and popular patches of the latter Cl.5 while it demonstrates by far the highest price intermittency and the least rapidly ageing population amongst suburban clusters. To sum up, the four multifractal parameters and the weighted mean of housing price combined—each representing a distinct property derived from the same dataset—were able to reconstruct the characteristic socioeconomic structure of the greater Paris region as also examined by previous research.

6. Conclusions

The overarching goal of the current study was to devise a methodology that is able estimate the so far hardly accessible *local multifractal parameters* in urban systems with *sufficing quality* independent from urban boundary constraints. It set out to do so separately for the spatial distribution (support) and any attached value (mark) in an attempt to fully understand the *roots of correlations* in the chosen spatial phenomena. In such way, it also aimed at minimising the effect of oftentimes strongly fluctuating data availabilities on the multifractal estimation of the mark in urban contexts. We demonstrated that the performance of the methodology is satisfactory both on synthetic and real-world data and results were highly consistent between the two. Moving on, the study on real-world housing purchases found that the four multifractal parameters (of support and mark combined) each hold distinct and complementary information: the low strength of correlations between them were indeed indicative of rather different structural properties within the same dataset. As an example, multifractal properties of the support corresponded with the behavior deduced in other natural phenomena where a weaker long-range dependency in the global sense (c_1) could be associated with higher extremes in local—in our case purchase—activity (c_2) [72] whereas for the mark we observed partly reversed tendencies. Generally, the multifractal parameters of housing price revealed the scarcely studied strength of correlations in local, neighbourhood-level structures that could be subsequently linked to concurrent variations in housing, economic and demographic inequalities. Along the same lines, the clustering analysis was able to recover the characteristic social, demographic and economic structure in the greater Paris region, also well-studied by previous research.

Outlook. We thus believe that the multifractal attributes of real estate values may be well combinable with other modeling attempts of housing price in the context of spatial economics however this remains for future research. An important restriction of this study consists in omitting observations on the temporal dynamics of the housing market, a highly relevant and interesting possible extension that certainly requires further methodological advancements. A natural progression of this work would be to analyze other geospatial systems where similar disentangling of the support and the mark could play an essential role, e.g. population distributions and their underlying urban morphology or street network pattern. Finally, a further study could assess applications in other inhomogeneous complex systems as described in detail in the introduction of this article.

Table A1. Coefficients of the multiple regression results for the three clusters within the municipal boundary of Paris. The dependent variable is defined as the multifractality of price $c_2(g)$ while explanatory variables are listed in the first row (p 0.001). Abbreviations: R.: Ratio, No.: Number, Soc. H.: Social Housing, H.h.: Households, EDI: Equivalised Disposable Income, I: Inhabitants.

	R. Under 18	No. Soc. H.	R. EDI/I.	R. Owner H.h.
Cl.1 ($R_2 = 0.825$)	−0.0602	0.0734	0.1175	−0.0950
Cl.2 ($R_2 = 0.872$)	−0.0798	0.0527	0.1715	−0.1681
Cl.3 ($R_2 = 0.706$)	−0.1184	0.0191	0.1883	−0.2466

Data availability statement

The data that support the findings of this study are available upon reasonable request from the authors.

Acknowledgments

Work supported by Projet Multifrac within the larger research framework I-SITE FUTURE in France.

Appendix A.

For the multiple regression analysis in section 5 we use four explanatory variables to predict the multifractality of price $c_2(g)$: the ratio of under-18 year-olds, the number of social housing units, the equivalised disposable income (EDI) per inhabitant and the ratio of ownership households. Data was collected from the micro-level census data [67]. Results for the three clusters within the municipal boundary of Paris are displayed in table A1.

ORCID iDs

J Lengyel https://orcid.org/0000-0002-1301-7907
S G Roux https://orcid.org/0000-0001-8561-1270
P Abry https://orcid.org/0000-0002-7096-8290
S Jaffard https://orcid.org/0000-0003-1671-0608

References

[1] Wendt H, Abry P and Jaffard S 2007 *IEEE Signal Process. Mag.* **24** 38–48
[2] Gerasimova E, Audit B, Roux S G, Khalil A, Gileva O, Argoul F, Naimark O and Arneodo A 2014 A wavelet-based method for multifractal analysis of medical signals: application to dynamic infrared thermograms of breast cancer *Int. Conf. on Nonlinear Dynamics of Electronic Systems* (Springer) pp 288–300
[3] Villain E, Wendt H, Basarab A and Kouamé D 2019 On multifractal tissue characterization in ultrasound imaging *2019 IEEE 16th Int. Symp. on Biomedical Imaging (ISBI 2019)* (Piscataway, NJ: IEEE) pp 1708–12
[4] Roux S, Arneodo A and Decoster N 2000 *Eur. Phys. J.* B **15** 765–86
[5] Drzewiecki W, Wawrzaszek A, Krupiński M, Aleksandrowicz S and Jenerowicz M 2019 Multifractal parameters in prediction of land-use components on satellite images *2019 Signal Processing: Algorithms, Architectures, Arrangements, and Applications* (IEEE) pp 296–301
[6] Lashermes B, Roux S G, Abry P and Jaffard S 2008 *Eur. Phys. J.* B **61** 201–15
[7] Robert R and Vargas V 2008 *Commun. Math. Phys.* **284** 649–73
[8] Friedrich J, Peinke J, Pumir A and Grauer R 2021 *J. Phys. Complex.* **2** 045006
[9] Carpineti M, Rossoni A, Senese A, Maragno D, Diolaiuti G A and Vailati A 2021 *J. Phys. Complex.* **2** 025003
[10] Ariza-Villaverde A B, Jiménez-Hornero F J and De Ravé E G 2013 *Comput. Environ. Urban Syst.* **38** 1–10
[11] Thomas I, Frankhauser P and Biernacki C 2008 *Landsc. Urban Plan.* **84** 99–115
[12] Pavón-Domínguez P, Ariza-Villaverde A B, Rincón-Casado A, de Ravé E G and Jiménez-Hornero F J 2017 *Comput. Environ. Urban Syst.* **64** 229–38
[13] Carbone A, Murialdo P, Pieroni A and Toxqui-Quitl C 2022 *J. Phys. Complex.* **3** 025007
[14] Sémécurbe F, Tannier C and Roux S G 2016 *Geogr. Anal.* **48** 292–313
[15] Vega Orozco C D, Golay J and Kanevski M 2015 *Cybergeo: Eur. J. Geogr.* 714
[16] Hu S, Cheng Q, Wang L and Xie S 2012 *Appl. Geogr.* **34** 161–70
[17] Lengyel J, Alvanides S and Friedrich J 2022 *Environ. Plan.* B
[18] Salat H, Murcio R, Yano K and Arcaute E 2018 *PLoS One* **13** e0196737
[19] Tannier C and Thomas I 2013 *Comput. Environ. Urban Syst.* **41** 234–48
[20] Hunt J, Eames I, Da Silva C and Westerweel J 2011 *Phil. Trans. R. Soc.* A **369** 811–32
[21] Neunaber I, Hölling M, Stevens R J, Schepers G and Peinke J 2020 *Energies* **13** 5392
[22] Kaimal J C and Finnigan J J 1994 *Atmospheric Boundary Layer Flows: Their Structure and Measurement* (Oxford: Oxford University Press)
[23] Molz F, Liu H and Szulga J 1997 *Water Resour. Res.* **33** 2273–86
[24] Engel A and Weigt M 1996 *Phys. Rev.* E **53** R2064

[25] Traphan D, Wester T T, Gülker G, Peinke J and Lind P G 2018 *Phys. Rev.* X **8** 021015
[26] Torre A and Darly S 2014 *Renew. Agric. Food Syst.* **29** 206–17
[27] Le Bivic C and Melot R 2020 *Land Use Policy* **99** 105040
[28] De Keersmaecker M L, Frankhauser P and Thomas I 2003 *Geogr. Anal.* **35** 310–28
[29] Hu S, Cheng Q, Wang L and Xu D 2013 *Landsc. Urban Plan.* **110** 25–35
[30] Baltagi B H, Bresson G and Etienne J M 2015 *J. Appl. Econ.* **30** 509–28
[31] Fingleton B 2008 *Urban Stud.* **45** 1545–63
[32] Leung C 2004 *J. Hous. Econ.* **13** 249–67
[33] Holmes M J, Otero J and Panagiotidis T 2017 *J. Real Estate Finance Econ.* **54** 1–16
[34] Taltavull de La Paz P and Gabrielli L 2015 *Hous. Stud.* **30** 1036–63
[35] Meese R and Wallace N 2003 *Urban Stud.* **40** 1027–45
[36] Baumont C and Legros D 2009 HAL Id: halshs-00579747 (accessed April 2022)
[37] Pace R K, Barry R, Clapp J M and Rodriquez M 1998 *J. Real Estate Finance Econ.* **17** 15–33
[38] Zhang Y, Zhang D and Miller E J 2021 *J. Urban Plan. Dev.* **147** 05021003
[39] Harding J P, Rosenthal S S and Sirmans C 2007 *J. Urban Econ.* **61** 193–217
[40] Goetzmann W N 1992 *J. Real Estate Finance Econ.* **5** 5–53
[41] Zietz J, Zietz E N and Sirmans G S 2008 *J. Real Estate Finance Econ.* **37** 317–33
[42] Nappi-Choulet I and Maury T P 2011 *J. Reg. Sci.* **51** 732–50
[43] Cui N, Gu H, Shen T and Feng C 2018 *Sustainability* **10** 4343
[44] Case B, Colwell P F, Leishman C and Watkins C 2006 *Real Estate Econ.* **34** 77–107
[45] Cerema, Demande de Valeurs Foncières 2022 https://cerema.app.box.com/v/dvfplus-opendata (retrieved January 2022)
[46] Eurostat, ec.europa.eu 2022 https://ec.europa.eu/eurostat/databrowser/product/page/ILC_MDED01__custom_2006550
[47] Reid J, Nicol C and Allen H 2019 (Deutsche Bank Research: Mapping the World's Prices) https://dbresearch.com/PROD/RPS_EN-PROD/PROD0000000000494405/Mapping_the_world
[48] De Palma A, Motamedi K, Picard N and Waddell P 2007 *Eur. Transp.* **36** 47–74
[49] Beaucire F and Saint-Gérand T 2004 *Built Environ.* **30** 111–5
[50] Brueckner J K, Thisse J F and Zenou Y 1999 *Eur. Econ. Rev.* **43** 91–107
[51] Fack G and Grenet J 2010 *J. Public Econ.* **94** 59–77
[52] Chapelle G, Wasmer E and Bono P H 2021 *J. Econ. Geogr.* **21** 97–126
[53] Górczyńska M 2017 *Hous. Stud.* **32** 385–410
[54] Chen Y and Wang J 2013 *Environ. Plan.* B **40** 884–904
[55] Tél T, Fülöp Á and Vicsek T 1989 *Physica* A **159** 155–66
[56] Mach J, Mas F and Sagués F 1995 *J. Phys. A: Math. Gen.* **28** 5607
[57] Vicsek T 1990 *Physica* A **168** 490–7
[58] Song Y Q, Liu J L, Yu Z G and Li B G 2015 *Sci. Rep.* **5** 17628
[59] Lengyel J, Roux S, Sémécurbe F and Jaffard S 2022 *Environ. Plan.* B https://doi.org/10.1177/23998083221116120
[60] Bacry E, Delour J and Muzy J F 2001 *Phys. Rev.* E **64** 026103
[61] Jaffard S, Seuret S, Wendt H, Leonarduzzi R and Abry P 2019 *Proc. R. Soc.* A **475** 20190150
[62] Muzy J F and Bacry E 2002 *Phys. Rev.* E **66** 056121
[63] Mandelbrot B B 1972 Possible refinement of the lognormal hypothesis concerning the distribution of energy dissipation in intermittent turbulence *Statistical Models and Turbulence* (Berlin: Springer) pp 333–51
[64] Robert R and Vargas V 2010 *Ann. Probab.* **38** 605–31
[65] Zhang H and Mei C 2011 *Int. J. Geogr. Inf. Sci.* **25** 1467–89
[66] Durning A 2021 *Sightline Institute* https://sightline.org/2021/07/26/yes-other-places-do-housing-better-case-3-paris/
[67] INSEE L'Institut national de la statistique et des études économiques 2015 INSEE Données carroyées—carreau de 200 m https://insee.fr/fr/statistiques/4176290?sommaire=4176305 (retrieved January 2022)
[68] Salvati L 2020 *Popul. Res. Policy Rev.* **39** 549–75
[69] Azière r and Goldgrab L 2019 Le périphérique, quelles perspectives de changements? *Tech. Rep.* (Ville de ParisConseil de Paris)
[70] Machline E, Pearlmutter D and Schwartz M 2018 *Build. Res. Inf.* **46** 636–52
[71] Fujita K and Maloutas T 2016 Segregation, social mix and public policies in Paris *Residential Segregation in Comparative Perspective* (*Cities and Society*) (New York: Routledge) pp 169–92
[72] La Rocca D, Zilber N, Abry P, van Wassenhove V and Ciuciu P 2018 *J. Neurosci. Methods* **309** 175–87